Effect of Grain Refinement on Jerky Flow in an Al-Mg-Sc Alloy

ANNA MOGUCHEVA, DIANA YUZBEKOVA, RUSTAM KAIBYSHEV, TATIANA LEBEDKINA, and MIKHAIL LEBYODKIN

The influence of microstructure on the manifestations of the Portevin–Le Chatelier (PLC) effect was studied in an Al-Mg-Sc alloy with unrecrystallized, partially recrystallized, and fully recrystallized grain structures. It was found that the extensive grain refinement promotes plastic instability: the temperature–strain rate domain of the PLC effect becomes wider and the critical strain for the onset of serrations decreases. Besides, the amplitude of regular stress serrations observed at room temperature and an intermediate strain rate increases several times, indicating a strong increase of the contribution of solute solution hardening to the overall strength. Moreover, the grain refinement affects the usual sequence of the characteristic types of stress serrations, which characterize the dynamical mechanisms governing a highly heterogeneous unstable plastic flow. Finally, it reduces the strain localization and surface roughness and diminishes the difference between the surface markings detected in the necked area and in the region of uniform elongation.

I. INTRODUCTION

IT is well known that the plastic flow of metallic alloys may become unstable within certain temperature and strain rate ranges, which is manifested as serrations on the stress–strain curve. This phenomenon, often denoted as jerky flow or repetitive yielding, is associated with heterogeneous localization of plastic deformation within the bulk of a material and is referred to as the Portevin-Le Chatelier (PLC) effect.[1–4] Al-Mg alloys present one of the widely used materials exhibiting this phenomenon.[4–7] The PLC effect is known to result in a reduction in ductility and the formation of deformation bands that leave undesirable traces on the surface of the sheet product.[5,6,8] The microscopic mechanism of this phenomenon is most often ascribed to dynamic strain aging (DSA), i.e., interaction of dislocations with solute atoms.[3–5,9–11] In particular, a recent atomic-scale investigation on an Al-4.3 pct Mg alloy proved that this interaction leads to segregation of Mg solute atoms on dislocations,[3] i.e., the formation of Cottrell clouds, under tension in the DSA regime.[4,5,12] Detachment of mobile dislocations from the solute atmospheres causes local softening and, hence, promotes slip localization

and planar slip. Besides the observations of strain localization in wide PLC deformation bands, which correspond to a millimeter scale, it is known that the initial microstructure influences the mesoscale topographical features and the surface roughness developed during plastic deformation.[8,13] However, there are little experimental data on the relationship between the initial microstructure, the PLC effect, and the surface markings. Therefore, examination of the effect of initial structure on the PLC instability is important for searching ways to improve the surface roughness and ductility impacted by plastic instability in industrial Al-Mg alloys.

The behavior of the PLC effect shows generic signatures depending on the strain rate and temperature. They are usually classified into three types according to the serration patterns and kinematics of the PLC bands. A more detailed nomenclature including five types was also proposed to discriminate some specific behaviors (Figure 1).[3–5] Type A serrations are distinguished as rises in the flow stress, followed by a drop to or below the general stress level (the so-called 'locking' serrations). They are observed at high strain rates or low temperatures and are associated with a repetitive continuous propagation of deformation bands, the flow stress rises marking the nucleation of a new band at an angle of ~60 deg to the tensile axis.[14,15] When the strain rate is decreased or temperature is increased, this behavior changes to type B serrations typically occurring about the general level of the stress–strain curve. An important signature of this type of instability is a hopping propagation of localized deformation bands. Type C behavior, characteristic of low strain rates or high temperatures, describes large stress drops below the general stress level (unlocking serrations), which are attributed to almost random nucleation of deformation

ANNA MOGUCHEVA, Senior Research Associate, DIANA YUZBEKOVA, Engineer, and RUSTAM KAIBYSHEV, Head, are with the Laboratory of Mechanical Properties of Nanostructural Materials and Superalloys, Belgorod State University, Pobeda 85, Belgorod, Russia 308015. Contact e-mails: mogucheva@bsu.edu.ru, annam08@mail.ru TATIANA LEBEDKINA, Research Fellow, and MIKHAIL LEBYODKIN, Head, are with the Laboratoire d'Etude des Microstructures et de Mécanique des Matériaux (LEM3), CNRS UMR 7239, Université de Lorraine, Ile du Saulcy, 57045 Metz, France.
Manuscript submitted November 5, 2015.
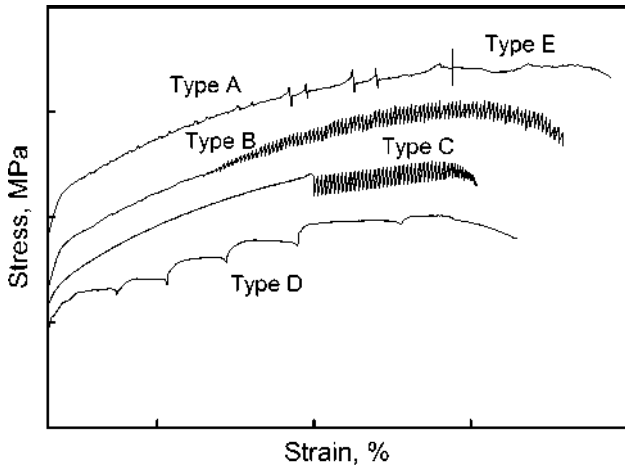Article published online February 24, 2016.

Fig. 1—Types of serrations (*cf.* Ref. [4]).

bands along the tensile axis.[16] Types *D* and *E* are associated with a continuous propagation of deformation bands but refer to less generic behavior than type *A*. Type *D* serrations appear as steps on stress–strain curves followed by plateaus with no work hardening. Type *E* serrations are usually distinguished at large strains and follow type *A* behavior. They are represented by irregular stress fluctuations with little or no work hardening during band propagation. These complex patterns attract much attention because the transitions between different types of discontinuous yielding are indicative of variations in the DSA mechanism and collective behavior of dislocations.[7,15,17]

So far, there is no consensus as to the effect of microstructural parameters, such as grain size, lattice dislocation density, and dispersion of secondary phase particles, on the PLC effect.[3,5,18–25] In particular, it was established that an extensive grain refinement or/and increase in the lattice dislocation density in dilute Al-Mg alloys, or similar alloys containing coarse particles of secondary phases, usually result in an increase in the critical strain ε_c for the onset of serrated flow and a decrease in the serration frequency and amplitude, up to effective suppression of the PLC effect together with strain hardening.[18–24] In contrast, the grain refinement was found to highly increase the magnitude of stress oscillations in an Al-Mg alloy containing non-shearable nanoscale particles.[26] These examples illustrate that the initial microstructure may affect the PLC phenomenon in radically different ways in dilute and dispersion hardened Al-Mg alloys. Indeed, while mobile dislocations are mainly blocked by forest dislocations in dilute alloys, precipitates are also effective obstacles in alloys containing nanoscale dispersoids.[27] The nature of obstacles is important for the arrest and detachment of mobile dislocations, so that Al-Mg alloys containing coherent dispersoids may exhibit distinctly different PLC behavior in comparison with dilute Al-Mg alloys.[28]

The aim of the present study was to realize a comprehensive study of the effect of grain refinement on serrated yielding in wide temperature and strain rate

ranges in an Al-Mg alloy containing a dispersion of nanoscale coherent particles of $Al_3(Sc,Zr)$ phase. Various microstructures were produced by equal channel angular pressing (ECAP) at 573 K (300 °C) to different strains, as described previously.[29] The paper is focused on the effects of microstructure on the temperature and strain rate domains of the PLC effect, the types of jerky flow, and the associated surface markings.[8]

II. MATERIAL AND EXPERIMENTAL PROCEDURE

The 5024 aluminum alloy with a chemical composition of Al-4.57Mg-0.35Mn-0.2Sc-0.09Zr (wt pct) was produced by continuous casting followed by hot extrusion.[26] The rods were pressed up to strains ~1, ~2, ~4, ~8, and ~12 *via* route B_C in which the samples are rotated by 90º along the same direction after each pass.[30] Other material and processing details were reported previously.[29]

Tensile specimens with a 16 mm gage length and 1.5×3 mm² cross section were cut parallel to the last extrusion axis of the pressed billets. Mechanical tests were carried out using an Instron 5882 testing machine at temperatures ranging from 173 K to 423 K (from −100 °C to 150 °C). The imposed strain rate was chosen in the range of 1×10^{-5} to 2.1×10^{-1} s⁻¹. The samples were held for about 10 minutes at the testing temperature in order to reach thermal equilibrium during the tests at elevated and subzero temperatures. The value of ε_c was calculated in a conventional way, as the minimum true strain value at which a visible stress fluctuation (≥1 MPa) appears on the stress–strain curve.

The surface analysis was realized using a scanning electron microscope (SEM) Quanta 600. Tensile specimens were initially mechanically polished and then electropolished using a solution of 25 pct HNO_3 + 75 pct CH_3OH. The surface topography was examined near the fracture tip and in the zone of uniform deformation of the specimens deformed to failure and to maximum stress (ε ~ 15 pct), respectively, at strain rates ranging from ~1×10^{-4} to ~2.1×10^{-1} s⁻¹ and temperatures ranging from 173 K to 373 K (from −100 °C to 100 °C).

III. EXPERIMENTAL RESULTS

A. *Deformation Microstructures*

The deformation structures produced by hot extrusion followed by ECAP in the 5024 alloy were described in detail in the companion work.[29] The microstructure obtained after hot extrusion consists of coarse grains elongated along the extrusion direction, with longitudinal and transverse dimensions ~200 and ~20 μm, respectively (Figure 2(a)). Nanoscale $Al_3(Sc,Zr)$ precipitates uniformly distributed in the bulk of material represent the main secondary phase.[26] ECAP up to a true strain ε of 1 or 2 resulted in the formation of a well-defined subgrain structure (Figure 2(b)). A partially
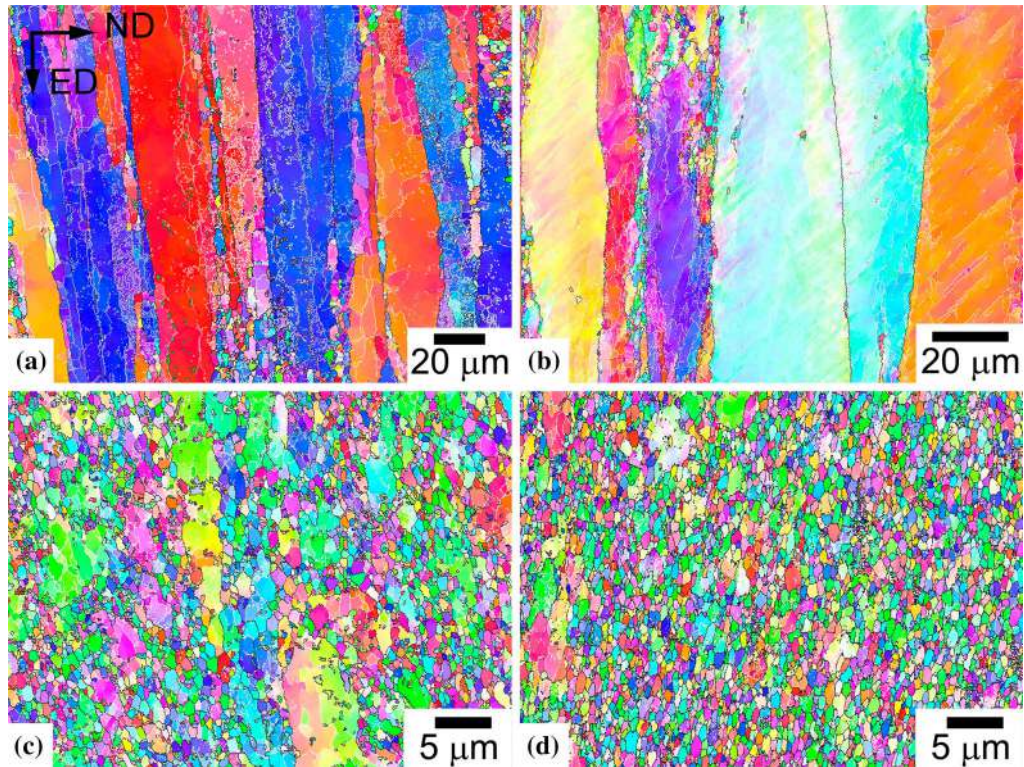
Fig. 2—EBSD misorientation map for the 5024 Al alloy in the initial as-received state (*a*) and deformed by ECAP to strains of (*b*) ε~1; (*c*) ε~4; (*d*) ε~12 (Color figure online).

Table I. Microstructural Characteristics of the AA5024

State	Grain Size (μm)	Fraction of Recrystallized Grains (pct)	θ (deg)	HAB's (pct)	Dislocation Density (m^{-2})
As-received	200/20	2	17.5	36.0	9.8×10^{12}
1 ECAP pass	17/10.6	2.4	12.6	23.0	5.0×10^{13}
2 ECAP passes	7.24/4.52	7	15.7	32.0	2.0×10^{14}
4 ECAP passes	1.33/1.16	54	26.4	62.0	1.4×10^{14}
8 ECAP passes	1.21/0.95	74	28.5	67.5	1.4×10^{14}
12 ECAP passes	1.01/0.88	86	30.0	70.4	1.2×10^{14}

recrystallized structure was obtained for ε ~ 4 or ~8 (Figure 2(c)) and a fully recrystallized structure for ε ~ 12 (Figure 2(d)). Table I summarizes the microstructural characteristics of the 5024 alloy in different conditions. The material subjected to ECAP displays a high density of lattice dislocations (Table I).[29] No effect of ECAP on the dispersion of Al₃(Sc,Zr) particles was found.[28]

B. Influence of ECAP on Jerky Flow at a Reference Temperature and Strain Rate

All deformation curves of the 5024 alloy tested at room temperature [298 K (25 °C)] and at strain rate of $\sim 1 \times 10^{-3}$ s^{-1} exhibit stress serrations, as illustrated in Figure 3, representing engineering σ-ε curves. The effects of the prior processing and the deformation stage on serration amplitudes at these reference conditions are summarized in Table II. The overall shape of the curves, the type of jerky flow, and the average

amplitude of serrations strongly depend on the prior microstructure (Table I and Figure 2). The coarse-grained material displays tensile curves typical of Al-Mg alloys, with an extensive initial strain hardening and an overall parabolic shape until necking, so that the maximum stress corresponds to a well-defined peak in the flow stress. Mixed type $A + B$ serrations take place during the strain hardening stage and the apparent 'steady state.'

Complex behavior consisting of a transition from mixed types $A + B$ during strain hardening stage to type B serrations during the apparent 'steady state' is displayed by the specimens subjected to 1 or 2 ECAP passes (Figure 3). The formation of a subgrain structure and an increase in the dislocation density (Table I) thus promote Type B serrations. Otherwise, it does not increase the yield stress but diminishes the strain hardening rate and, consequently, the peak stress. Surprisingly, it is accompanied by an increase in ductility. Moreover, when the flow stress achieves the
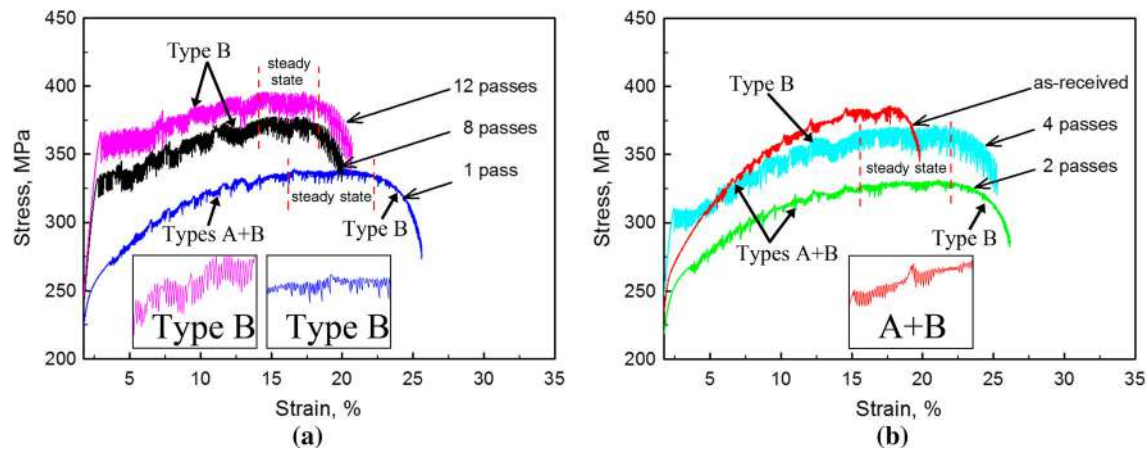
Fig. 3—Typical stress–strain curves for the 5024 alloy before and after ECAP, obtained at a strain rate of 1×10^{-3} s^{-1} at 298 K (25 °C) (*a*, *b*) (Color figure online).

Table II.   Effect of Number of ECAP Passes and Strain on the Amplitude Range (MPa) of Stress Oscillations at the Reference PLC Conditions

	Amplitudes		
State	~1 to 3 pct	~12 to 14 pct	~16 to 17 pct
As-received	3	6	4
1 ECAP pass	3	5	4
2 ECAP passes	4	5	4
4 ECAP passes	13	16	20
8 ECAP passes	14	15	18
12 ECAP passes	20	17	21

The numbers of percents indicate the strain intervals corresponding to the estimates.

maximum, it remains at approximately the same level for a relatively extended apparent 'steady-state' period before the necking occurs. The aforementioned transition to pure type *B* serrations occurs in the vicinity of the peak stress. Their amplitude tends to diminish during necking.

The formation of a partially or fully recrystallized structure in samples subjected to 4 or 8/12 ECAP passes, respectively, results in a transition to a different kind of mechanical behavior. The qualitative features are similar in both cases. First, the formation of submicron-scale grains progressively increases the yield stress. After the elastoplastic transition, the deformation curves exhibit a plateau superimposed with high-amplitude serrations of type *B*, which can be seen as high-amplitude and frequency oscillations between upper and lower yield strengths.[31] This mechanical behavior could be interpreted in terms of a Piobert–Lüders plateau, taking into account that the difference between the upper yield strength and the lower yield strength is equal to the amplitude of serrations.[31–33] When the fraction of recrystallized grains grows (Table I), both the upper and the lower yield strengths increase (Table II), and the yielding plateau becomes longer. The subsequent strain hardening is less pronounced than in the cases of the coarse-grained material and the alloy subjected to 1 or 2 passes and characterized by a well-defined

substructure.[29] More precisely, the amount of strain hardening gradually reduces when the volume fraction of micron scale grains increases. In all cases, an apparent 'steady state' at the maximum stress is observed before necking. The highest ductility value only persists after 4 passes and is reduced after a more severe processing. Nevertheless, it is noteworthy that even in the last case, the ductility remains close to its value in the coarse-grained state. Finally, deep type *B* serrations are observed in each case all over the deformation curve. It is noteworthy that beyond the initial yielding plateau, they follow a staircase envelope σ-ε curve till the maximum stress. Regular stress oscillations of type *B* around a smooth envelope curve appear during the 'steady' stage and necking.

Second, the extensive grain refinement significantly increases the magnitude of stress drops, which contrasts with the behavior of dilute Al-Mg alloys or similar alloys containing coarse particles of secondary phases.[18–24] It can be seen that the average amplitude varies around 5 MPa in the coarse-grained state and after one or two ECAP passes and around 20 MPa after 12 passes of ECAP (Table II). In the alloy with a partially or fully recrystallized structure, the amplitude of serrations is nearly independent of strain, while in the coarse-grained state, the amplitude increases by a factor of 2 from the yield point to the peak stress and then
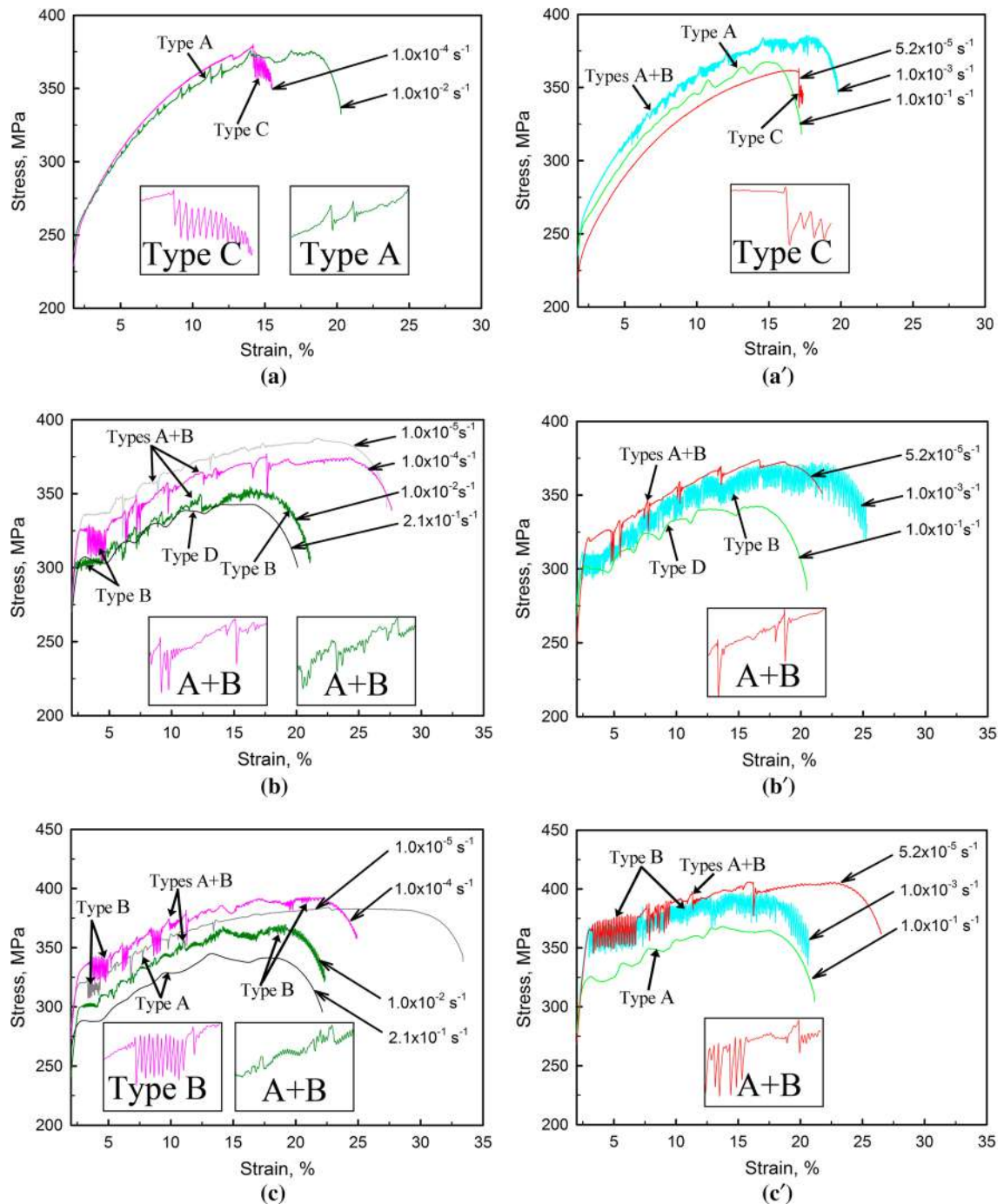
Fig. 4—Stress–strain curves obtained at room temperature and different strain rates: (a, a')—as-received 5024 alloy; (b, b')—after 4 ECAP passes; (c, c')—after 12 passes (Color figure online).

tends to decrease. Since the stress drop size is a measure of the solute contribution to strengthening through the DSA mechanism,[20,26] it can be concluded that the formation of recrystallized structures increases this contribution by a factor of 3 and more, depending on the recrystallized fraction in microstructure and the deformation stage (Table II). However, twenty-fold increase in dislocation density after 2 passes of ECAP (Table I) has no effect on the amplitude of serrations (Table II).

C. Influence of Strain Rate and Temperature on Serrations

Figures 4, 5, and 6 present the σ-ε curves obtained in a wide range of strain rate (1×10^{-5} s^{-1} to 2.1×10^{-1} s^{-1}) and temperature ranging from 223 K to 323 K (from -50 °C to 50 °C) for the 5024 alloy in the coarse-grained state and with partially and fully recrystallized structure after 4 and 12 passes of ECAP, respectively. At a strain rate of 1×10^{-3} s^{-1}, jerky flow
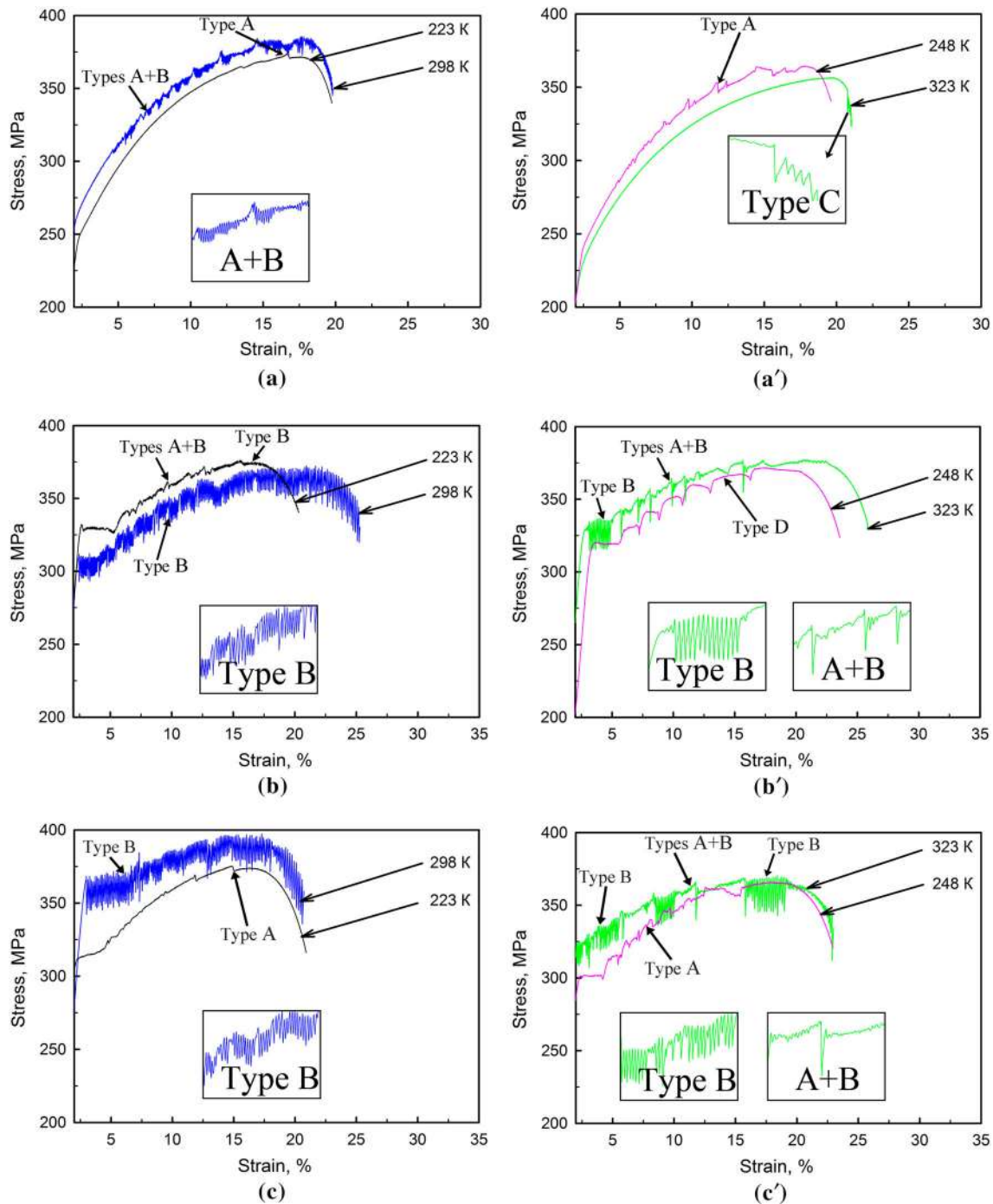
Fig. 5—Stress–strain curves obtained at a strain rate of 1×10^{-3} s^{-1} in the temperature range of 223 K to 323 K (-50 °C to 50 °C): (a, a′)—as-received 5024 alloy; (b, b′)—after 4 ECAP passes; (c, c′)—after 12 passes (Color figure online).

occurs in the temperature interval 223 K to 323 K (from -50 °C to 50 °C) for all material conditions, while smooth deformation curves are observed both below and above this interval, thus indicating the temperature domain of instability (Figures 4, 5, and 6). At ambient temperature, both the lower and upper strain rate boundaries of the PLC domain are found for the coarse-grained material (Figures 7(a) and 8(a)). In particular, it is shown in Figure 4(a′) that the onset of

stress serrations practically coincides with rupture at 5.2×10^{-5} s^{-1}. The extensive grain refinement noticeably expands the strain rate domain of instability: jerky flow is found in the entire range from 1.0×10^{-5} s^{-1} to 2.1×10^{-1} s^{-1} (Figures 4(b, b′) and (c, c′), 7(b) and (c), 8(b) and (c)).

As can be recognized in Figures 4(a, a′), 5(a, a′), 7(a), and 8(a), the coarse-grained material displays a conventional sequence of types A, $A + B$, and C when the strain
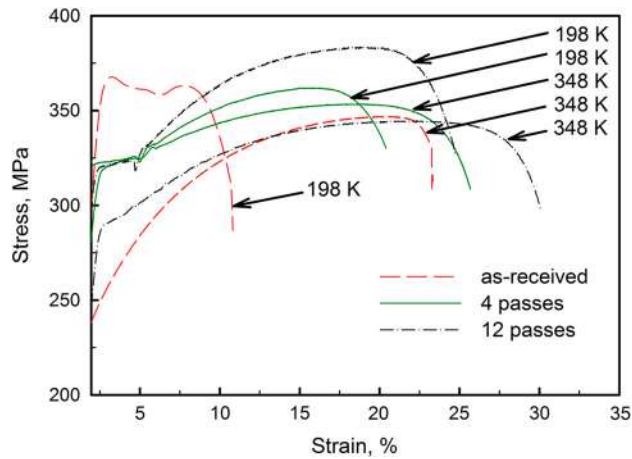
Fig. 6—Smooth stress–strain curves obtained at a strain rate of 1×10^{-3} s^{-1} and temperatures near the border of the PLC instability domain.

rate or temperature is decreased or increased, respectively. It should be specified that types *A* and *B* dominate the overall pattern, whereas type *C* serrations are only observed during short periods at the stage of necking at the left (low strain rate/high temperature) boundary of the PLC domain.

The extensive grain refinement changes the habitual sequence of serration types. Let us first consider the material subjected to 4 ECAP passes (Figures 4(b, b′), 5(b, b′), 7(b), and 8(b)). As described in Figure 3, deep type *B* oscillations are expectedly observed for the reference conditions (298 K (25 °C) and $\dot{\varepsilon} = 10^{-3}$ s^{-1}) which correspond to the middle part of the temperature and strain rate domain of the PLC effect (Figures 7(b) and 8(b)). Surprisingly, a deviation from these conditions toward any domain boundary (and not only toward higher $\dot{\varepsilon}$ or lower *T*) is accompanied with a tendency to either type *A* or *D* serrations corresponding to continuous propagation of deformation bands, even if type *B* displays persistence and gives rise to mixed $A + B$ behavior on either side of the reference conditions (Figures 7(b) and 8(b)). Far from the left and right boundaries of the PLC domain, type *B* serrations can be superimposed on $A + B$ behavior and mainly persist on the yielding plateau and on the late stage of deformation (Figures 4(b′) and 5(b)). They display large amplitude at 323 K (50 °C) (Figure 5(b′)) and 10^{-4} s^{-1} (Figure 4(b)) and disappear abruptly when the deformation conditions move sufficiently far from the reference ones. In the latter case, their amplitude is reduced progressively. Close to the left and right boundaries of the PLC domain (Figure 8(b)), mixed type $A + B$ and pure *A* serrations are observed up to necking (Figures 4(b, b′) and 5(b, b′)). Type *C* behavior, indicative of static bands, does not occur.

Figures 4(c, c′) and 5(c, c′) present similar families of σ-ε curves after ECAP to $\varepsilon \sim 12$. The comparison with the curves of Figures 4(b, b′) and 5(b, b′) shows that the effect of temperature and strain rate on the jerky flow in the material with partially and fully recrystallized structure is nearly the same. In this case too, a tendency
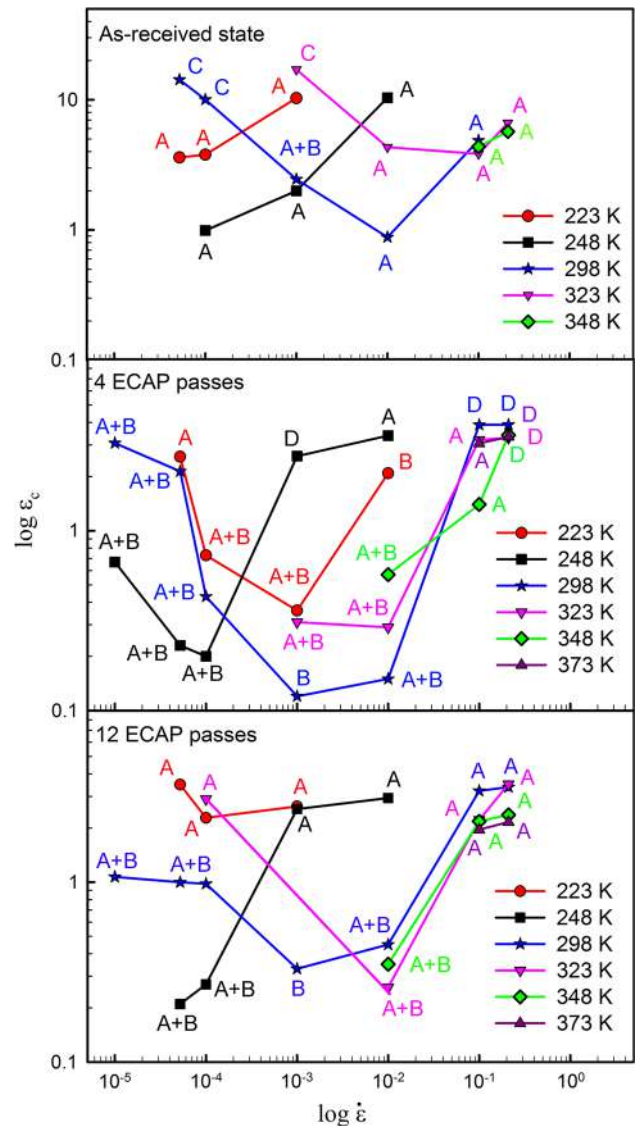

Fig. 7—The effect of (*a–c*)—strain rate and temperature and (*d*)—grain size on the critical strain ε_c.

to serration types corresponding to propagation of deformation bands is observed when approaching any border of the PLC domain (Figures 7(c) and 5(c)). However, some differences can be revealed. First, type *B* serrations become much more persistent, and their amplitudes slightly increase (Table II). On the yield plateau, in particular, they tend to vanish progressively close to the high *T* or low $\dot{\varepsilon}$ borders of the PLC domain (Figures 4(c, c′), 5(c′), and 8(c)). Such proneness to type *B* gives rise to particular behavior at 323 K (50 °C) and $\dot{\varepsilon} = 10^{-3}$ s^{-1} (Figure 5(c′)). In this case, deep type *B* serrations occur through the whole test in windows alternating with windows of type $A + B$ behavior (Figure 5(c′)). Another difference with the partially recrystallized material consists of a much weaker tendency to the type *D* staircase, which gives place to type *A* behavior (Figures 4(c, c′), 5(c, c′), 7(c), and 8(c)).

As far as type *D* serrations are concerned, they are observed at the upper boundary of the PLC domain, *i.e.,*

at high strain rates $\dot{\varepsilon} \geq 1 \times 10^{-1}$ s^{-1} and 298 K (25 °C) (Figure 4(b, b′)), in the alloy with a partially recrystallized structure only (Figures 7(b) and 8(b)). Type D is also observed at 248 K and reference strain rate, but this effect of temperature does not seem to be a rule because the behavior again changes to type $A + B$ at 223 K (−50 °C) (Figures 5(b, b′)). Apparently, in the alloy with a partially recrystallized structure, type A may be substituted by type D, which is in fact a variety of type A as it was shown above, with increasing the strain rate or decreasing temperature (Figures 7(b) and 8(b)). It can be suggested that the tendency to type D behavior at high strain rates is one of the specific features of the mixed microstructure formed after 4 ECAP passes. It should be recalled that such behavior means that the propagation of deformation bands along the tensile axis of the specimen takes place without strain hardening, but repetitive propagation occurs in the hardened specimen.

D. *Critical Strain and Activation Energy*

The effect of temperature and strain rate on the critical strain ε_c for the onset of serrations is illustrated in Figure 7. The types of PLC behavior immediately after its onset are indicated for all data points in Figure 7, as well as for the points close to the boundaries of the PLC domain in Figure 8. At 298 K (25 °C), the strain rate dependence of ε_c displays well-known non-monotonic behavior referred to as 'normal' in the range of high $\dot{\varepsilon}$ (ε_c increases with an increase in $\dot{\varepsilon}$) and 'inverse' (decreasing ε_c) in the opposite limit.[34,35] The minimum of the dependence corresponds to 10^{-2} s^{-1} in the coarse-grained state and 1×10^{-3} s^{-1} after several ECAP passes. The upper plot illustrates the temperature effect for the coarse-grained material. The main trend can be depictured as if the ε_c *vs* $\dot{\varepsilon}$ dependence was shifted as a whole to the left (toward lower $\dot{\varepsilon}$), when T was decreased from ambient temperature to 223 K (−50 °C). Consequently, only the 'normal' branches of the dependences are seen at 248 K and 223 K (−25 °C and −50 °C), their 'inverse' counterparts finding themselves beyond the lower strain rate boundary of the PLC domain. In a similar way, the ε_c *vs* $\dot{\varepsilon}$ dependence seems to shift to the right at higher T, so that mostly the 'inverse' branch remains present at 323 K (50 °C). It should be noted that a short normal branch is also seen on the latter curve, but it is stuck to the normal branch of the reference curve, as well as the ε_c values found at 348 K (75 °C).

The formation of a recrystallized structure promotes plastic instability in the present alloy by slightly extending both its temperature and strain rate domain toward the boundaries observed for dilute Al-4.7Mg alloys.[32–34] The critical strain is reduced by an order of magnitude after ECAP (Figure 7). The values ε_c obtained for the AA5024 alloy with both partially and fully recrystallized structure (Figures 7(b) and (c)) are less than those reported for other Al-4.7Mg alloys.[32,34] The effect of T and $\dot{\varepsilon}$ on ε_c observed after ECAP is more difficult to systematize. On the one hand, the ε_c *vs* $\dot{\varepsilon}$ dependence shifts to the left when T is reduced from
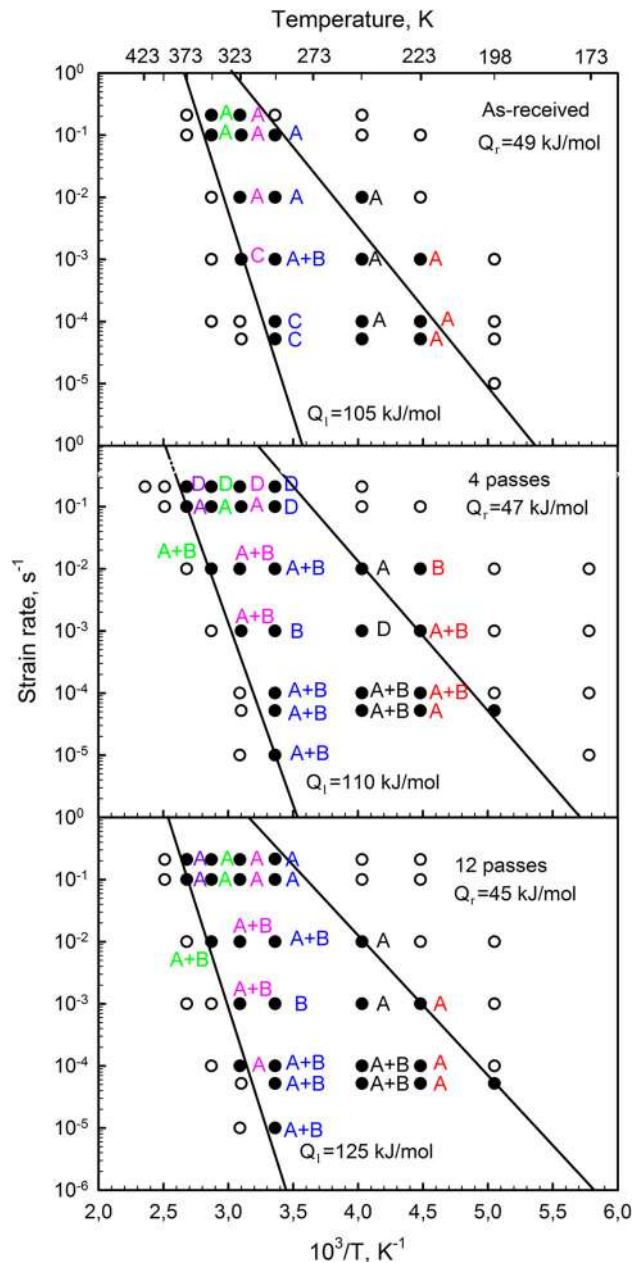

Fig. 8—Strain rate *vs* temperature domains of serrated flow in the 5024 alloy. (a) as-received state; (b) after 4 ECAP passes; (c) after 12 ECAP passes (open symbols: no serrations, closed symbols: serrations) (Color figure online).

298 K to 248 K (25 °C to −25 °C), thus confirming the trend described above for the coarse-grained material. On the other hand, a backward shift is observed upon decreasing temperature down to 223 K (−50 °C) for the specimen subjected to four passes. In most cases, only normal behavior was found for high temperatures (except for 323 K (50 °C), 12 passes). All these normal branches are stuck to the reference ε_c *vs* $\dot{\varepsilon}$ dependence for 298 K (25 °C).

Figure 8 quantifies the above qualitative conclusions as to the expansion of the (T, $\dot{\varepsilon}$) domain of the PLC effect after ECAP. It is clearly seen that for each $\dot{\varepsilon}$, the

temperature interval of instability extends slightly both to low-T and high-T regions, as shown by the delimiting boundaries between stable and unstable behavior. Such boundaries can be described by the following equation according to Cottrell theory[36]:

$$\dot{\varepsilon} = \frac{4b\rho C_{v}D_0}{l}\exp\left(\frac{-Q}{\kappa T}\right), \qquad [1]$$

where b, ρ, C_{v}, D_0, l, Q, and κ represent the Burgers vector, the dislocation density, the vacancy concentration, the diffusion frequency factor, the effective radius of the solute atmosphere, the activation energy for solute migration, and the Boltzmann constant, respectively.

The slopes of these dependences in the $\ln\dot{\varepsilon} - 1/T$ plots in Figure 8 allow for evaluating the apparent activation energy of serrated yielding. The estimates show a gradual decrease in the Q_r value found for the right boundary, from 49 kJ/mol in the coarse-grained state to 45 kJ/mol in fully recrystallized condition, and a respective increase in the value for the left boundary, Q_l, from 105 to 125 kJ/mol. The microstructure effect on the Q values for the right and left boundaries is consistent with the aforementioned changes in the serrations types (Figure 8). Indeed, there is no significant effect of the formation of a recrystallized structure on the serration type near the right boundaries, in agreement with the weak dependence of Q_r on the number of ECAP passes. In contrast, a well-defined transition from pure type A or C serrations to mixed type $A + B$ serrations occurs near the left boundary (Figure 8), in consistence with a significant increase in the Q_l value.

The unequal activation energies for the left and right boundaries indicate that they are controlled by different microscopic mechanisms. This is usually ascribed to the difference between the unlocking character of type C serrations near the left boundary of the domain of instability and the locking character of type A serrations near the right boundary. In the present case, such interpretation is only valid for the coarse-grained alloy at $\dot{\varepsilon} \leq 10^{-3}$ s^{-1} (Figure 8(a)), whereas in the alloy with partially or fully recrystallized structure, the left boundary of the instability domain is associated with mixed type $A + B$ serrations, which are replaced by pure type A serrations at the right boundary (Figures 8(b) and (c)). This observation agrees with the present-day understanding that the DSA mechanism alone cannot describe the complexity of the PLC effect but requires taking into account the spatial coupling within a heterogeneously deformed material, the latter is controlled by the microstructure.[7,15,23,37]

E. The Surface Topography

Similar to most of the literature (*e.g.,* References 8,38 through 40), the presented analysis was concentrated on a mesoscopic scale (tens or hundreds μm) that is usually associated with the inherent grain-scale roughening behavior, or 'orange-peel' effect. The surface features resulting from plastic deformation were found to be strongly dependent on grain size and necking, while less

dependent on temperature and strain rate. Figure 9 presents typical surface topography for the coarse-grained state. At ambient temperature and strain rate of 1×10^{-2} s^{-1}, coarse markings indicating a strong localization of dislocation glide occur in the necked region (Figures 9(a, a')).[8,41–43] Slip lines are organized in coarse slip bands giving rise to stair-step features.[43] At least, two independent slip systems are clearly seen in almost all elongated grains, although one slip system is preponderant. Most of slip bands are inclined at an angle of 45 deg to the tensile axis, which corresponds to the nearly maximum shear stress, *i.e.,* appear in grains having two slip systems with high Schmid factors.[40] In contrast to other observations of Al alloys,[8,38–40,43] the slip traces arriving at the longitudinal boundaries of elongated grains are continued in the neighboring grains almost without deviation, which might testify to propagation of slip bands through such boundaries. Slip transfer across special $\Sigma 3 \div \Sigma 11$ boundaries may occur in *fcc* metals through their crossing by dislocations assisted by stress concentration at the tip of the in-going dislocation pile-up.[44] However, the fraction of CSL (coincidence site lattice) boundaries in the 5024 alloy is negligible in any conditions.[29] It can be suggested that in the present material the slip transmission occurs through the dislocation emission from a high-angle boundary containing extrinsic dislocations.[45,46] Strain localization promotes this process, while segregations of solute atoms significantly increase the critical stress required to eject dislocations from a grain boundary.[45–47]

The slip bands inclined at much higher angles deviate significantly when crossing the grain boundaries. This deviation depends on the crystallographic orientation of the adjacent grains and is fitted by a wavy slip (Figure 9(a)). The high magnification used in Figure 9(a') shows that the wavy slip is related to interweaving patterns of stepped slip lines which testify to cross-slip mechanism.[41] Therefore, the cross-slip provides an accommodation mechanism for plastic flow through the boundaries between differently oriented grains. It is apparent that slip localization in a grain with relatively low Schmid factors may induce localized slip in a neighboring grain.

In the zone of uniform deformation the slip bands are rarely observed, while valleys and hills (*cf., e.g.,* Reference 40) are developed (Figure 10). One slip system is usually dominant (Figure 10). In general, surface markings are poorly defined and resemble slip lines in an AA5754 alloy deformed by tension to nearly the same strain.[8] On the whole, there is a correspondence between the necking in the coarse-grained material, on the one hand, and strong localization of multiple slip and stair-step nature of the sample surface, on the other hand. It is obvious that necking induces multiple slip and results in a strong strain localization.

The decrease in temperature at the same strain rate promotes the localization of the dislocation slip in coarse features and hinders the cross-slip and the propagation of slip bands through grain boundaries (Figure 9(b, b')). Slip lines having different orientations in neighboring areas are joined, which leads to the
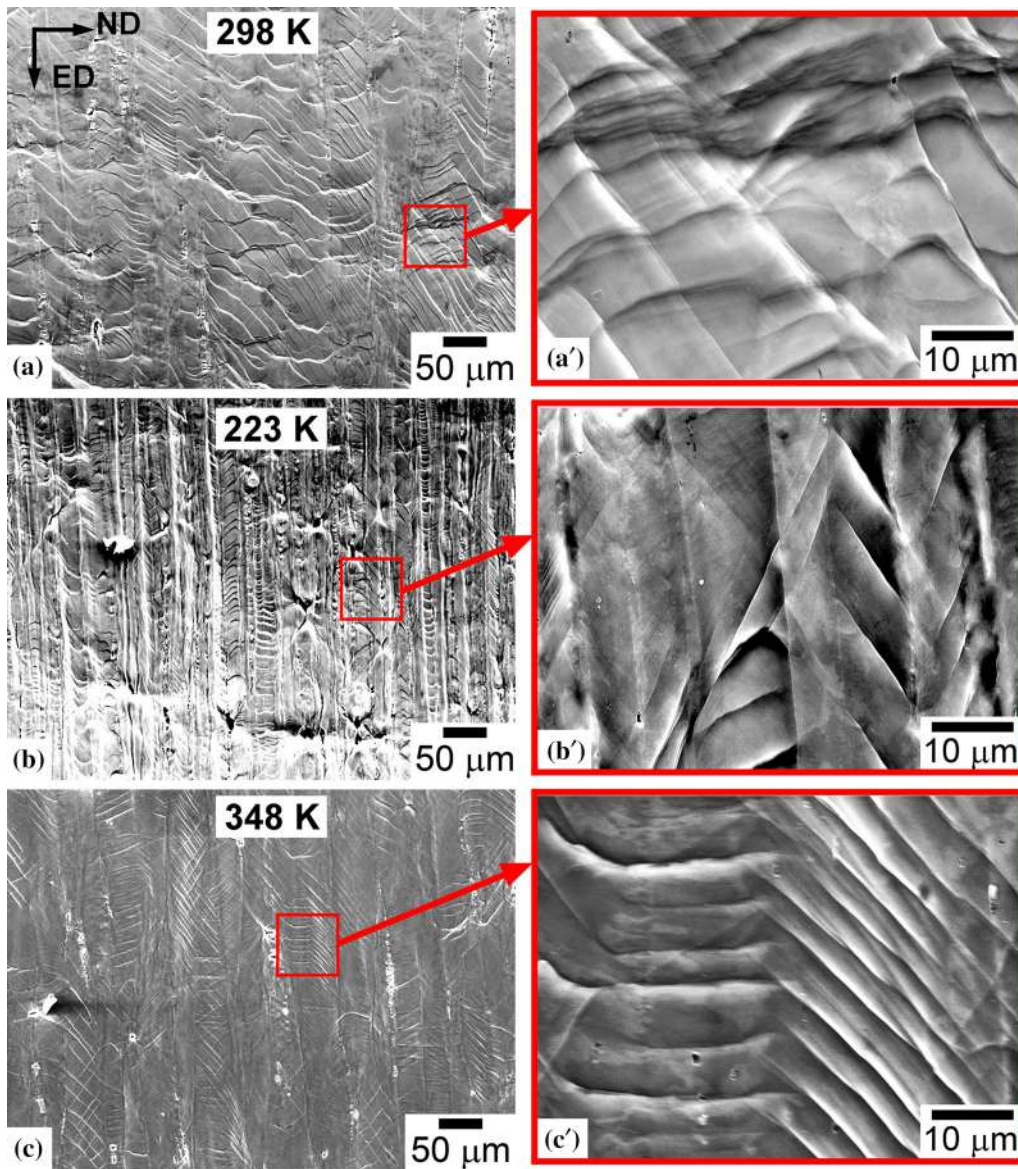
Fig. 9—Surface topography of tensile specimens cut from the as-received 5024 alloy and deformed at 1×10^{-2} s^{-1} and different temperatures: (a, a′) 298 K (25 °C); (b, b′) 223 K (−50 °C); (c, c′) 348 K (75 °C) (Color figure online).

development of ridges in the tension direction.[43] The increasing temperature diminishes the slip localization, facilitates the cross-slip, and also hinders the slip propagation through grain boundaries (Figures 9(c, c′)). No stair-step features were observed in this case, so that the sample surface containing coarse slip tended to become nearly flat (Figures 9(c, c′)). It is likely that the passing of slip lines through a grain boundary is facilitated at deformation conditions corresponding to the minimum in ε_c value (cf. Figure 7).

The formation of partially or fully recrystallized structures in the 5024 Al alloy highly increases the uniformity of dislocation glide and decreases the surface roughness, as can be viewed in Figures 11(a) and 12(a), respectively. It is obvious that glide occurs in all grains, but the surface features are unresolvable within fine grains even at a very high magnification (Figures 11(b)

and 12(b)). Evidence of slip features within recrystallized grains was found only at low temperatures (Figure 12(c)) or high strain rates (Figure 12(d)). The necking promoted the formation of coarse slip bands and multiple/cross-slip within the remnant of initial grains (Figures 11(c) and (d)).[29] However, no significant effect of necking on the surface roughness in zones with ultra-fine grains was found. It should be noted that the surface topography shown in Figures 12(c) and (d) resulted from plastic deformation at 173 K and 373 K (−100 °C and 100 °C) and strain rates 1×10^{-2} and $2.1 \times 10^{-}$ s^{-1}, respectively, corresponding to smooth deformation curves in the absence of jerky flow. Therefore, the uniformity of the dislocation glide in the alloy with recrystallized structure is higher within the PLC domain than outside of this domain (Figure 12), in contrast with the results for the coarse-grained alloy

(Figure 9). No passing of coarse slip bands through the boundaries of such grains was detected (Figures 11(a) and 12(a)). Figures 12(c) and (d) bear evidence that single slip is dominating within the recrystallized grains.

Furthermore, the grain refinement leads to an increase in the density of slip bands with decreasing the strain rate, in the same manner as in a coarse-grained Al-Mg

Fig. 10—Surface topography in the region of uniform elongation of specimens cut from the as-received 5024 alloy and deformed to maximum stress ($\varepsilon \sim 15$ pct). Tensile tests were carried out at 1×10^{-3} s^{-1} and 298 K (25 °C).

alloy studied by Kang et al.[42] Indeed, in the coarse-grained state, the slip bands are located at a distance of 5 to 10 μm from each other. Figures 11(a) and 12(a) testify that this distance decreased to 2 to 3 μm in the remnants of the coarse grains and to ~1 μm in fine-grained regions, respectively. Therefore, the formation of a fine-grained microstructure in the 5024 alloy resulted in a significant slip delocalization as compared to the coarse-grained material.

Finally, the analysis of the entirety of data bears evidence that type A serrations correlate with the dislocation slip propagating through grain boundaries, whereas such propagation is not observed after deformation governed by type B serrations.

IV. DISCUSSION

It is well known (e.g., References 4, 12, 48, and 49) that there exist critical deformation conditions, i.e., strain, strain rate, and temperature, for the occurrence of the PLC effect. These control parameters strongly affect the characteristics of jerky flow. The present results prove that the grain structure and a dispersion of secondary phase particles are also important control parameters for the PLC effect. First of all, it is worth noting that the temperature–strain rate PLC domains of the AA5024 alloy in coarse-grained condition (Figures 7(a) and 8(a)) are similar to those found for Al-4.5Mg alloys containing a dispersion of incoherent
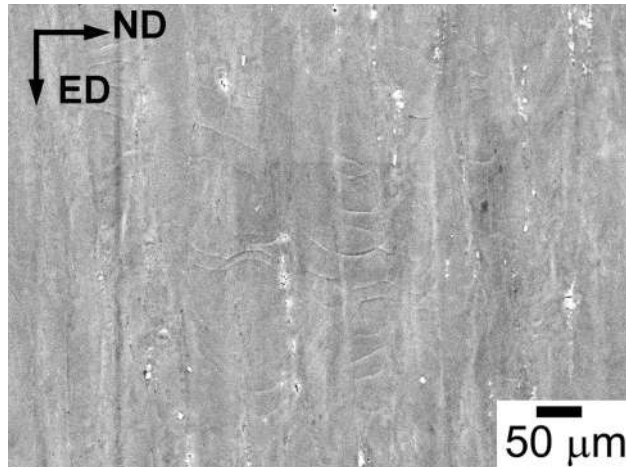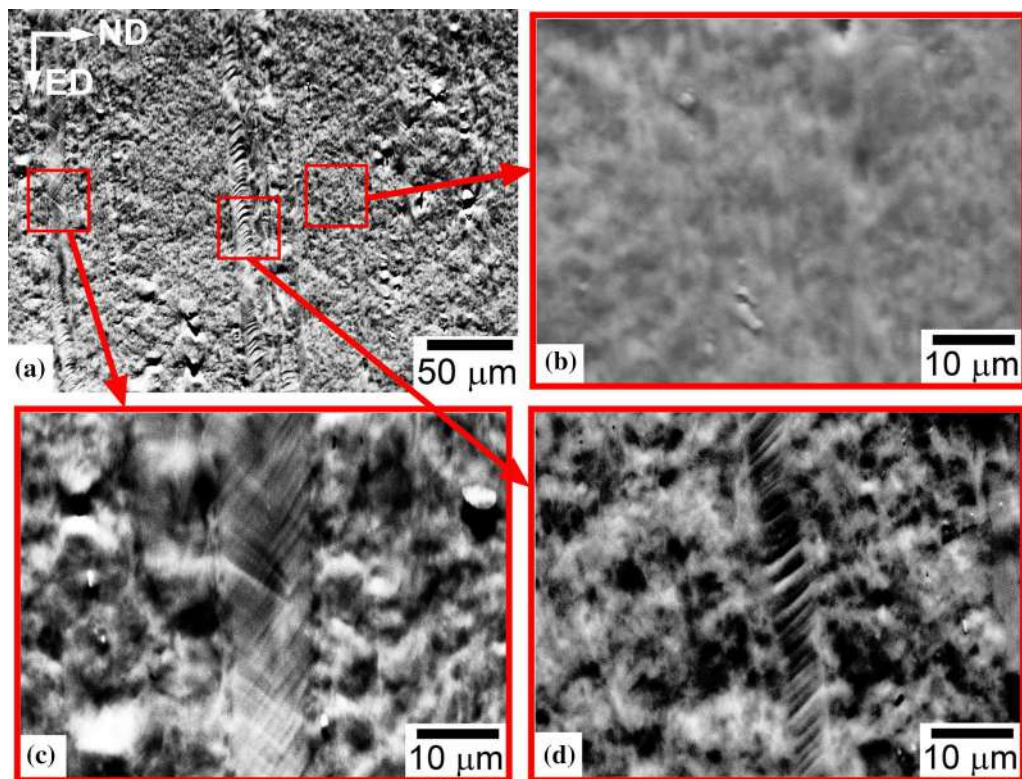

Fig. 11—Surface topography of tensile specimens cut from the 5024 alloy subjected to 4 ECAP passes. Tensile tests were carried out at 1×10^{-2} s^{-1} and 298 K (25 °C) (Color figure online).
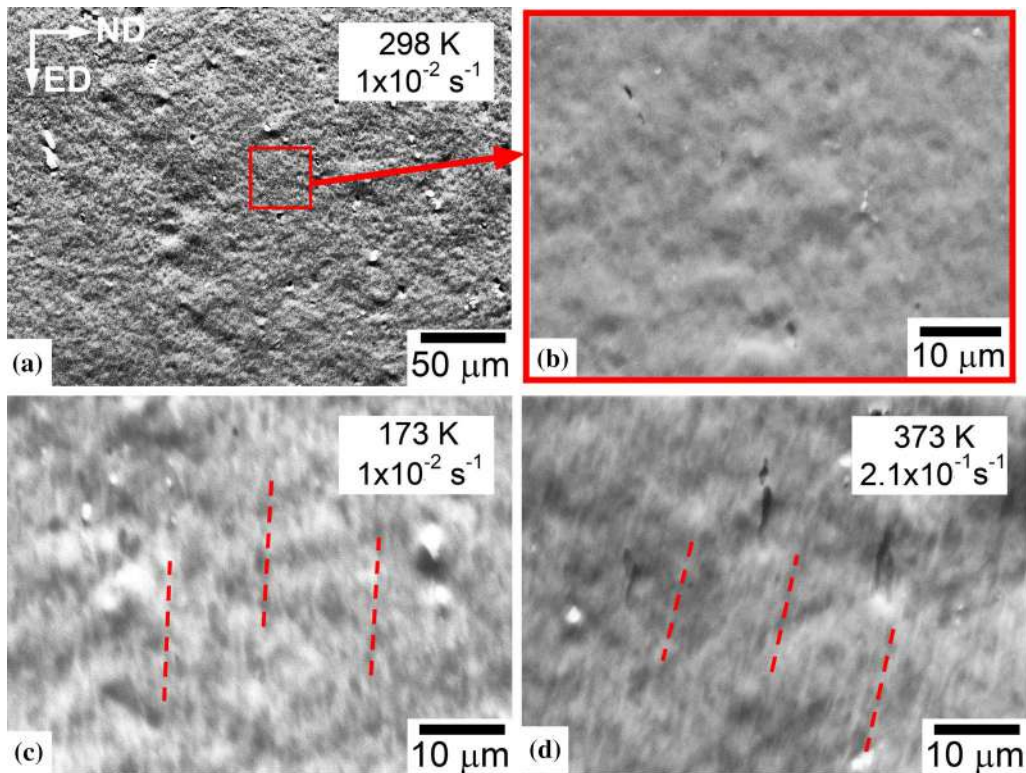
Fig. 12—Surface topography of tensile specimens deformed after 12 ECAP passes at different strain rates and temperatures. Photographs (*a*) and (*b*) illustrate the overall uniformity of the specimen surface. Diffuse slip traces can be recognized in (*c*) and (*d*), as exemplified by dashed lines (Color figure online).

secondary phases.[50–52] A dilute Al-4.8Mg alloy exhibits a slightly expanded PLC domain.[35] Furthermore, in contrast to other Al-4.7Mg alloys,[50,51] pure type *B* behavior was not found at any temperatures and strain rates within the PLC domain, except for large strains corresponding to the apparent 'steady-state' jerky flow (Figures 4(a, a′), 5(a, a′) and 7(a)). It can be suggested that the dispersion of coherent nanoscale Al$_3$(Sc,Zr) particles impedes the 'hopping' behavior and gives rise to a transition from type *B* serrations to mixed type *A* + *B* within the PLC domain (*cf*. Reference 28). Indeed, it is known that these dispersoids are effective pinning centers for gliding dislocations.[6,53] This transition is accompanied with some decrease in the work hardening rate dσ/dε. As a result, the 5024 alloy exhibits a lower work hardening than other Al-4.7Mg alloys at all strain rates.[36,54] This unexpected fact is likely to be related to the three-fold increase of the yield stress caused by the presence of coherent dispersoids in the Al-Mg solid solution. Finally, the extensive grain refinement leads to a further decrease in the work hardening (Figure 3).

As far as the effect of the grain structure is concerned, a 20-time increase in the dislocation density (Table I) after two ECAP passes weakly affects the qualitative characteristics of tensile behavior and the PLC domain (Figure 3), similar to the data for a dilute Al-4.3 pct Mg.[3] In general, at high lattice dislocation density, the solute concentration may become insufficient to lock most of the dislocations and the PLC effect may disappear completely.[27] However, in the present case,

only quantitative changes take place owing to the increasing dislocation density. At the same time, the grain refinement (4 to 12 ECAP passes) drastically modifies mechanical behavior and uniformity of dislocation glide, indicating that the processes associated with the DSA mechanisms[4,11–14] depend on the grain size (Figure 8). In addition, it was found to increase the solid solution hardening, attributed to DSA and associated with the amplitude of stress serrations,[26,55] by a factor about 4 (Table II). With this point in view, it should be noted that the grain refinement strongly influences the dynamical mechanisms of plastic instability, through its effect on the localization of dislocation glide, the number of the dislocation slip systems operating within one grain, and the feasibility of the cross-slip. This influence is likely responsible for the effect of the microstructure on the critical strain ε_c, the serration types, and the PLC domain. The initial microstructure also has a strong impact on the process of propagation of the dislocation glide from one grain to another.

Importantly, it is shown that the character of the influence of microstructure on the PLC phenomenon strongly depends on the dispersion of second-phase particles. Indeed, the extensive grain refinement through intense plastic straining was earlier found to suppress stress serrations, as reported, *e.g.,* for a dilute Al-3 pct Mg alloy[23] or an Al-6 pct Mg alloy containing coarse plate-like particles of an Al$_6$Mn-phase.[22] In the present work, the extensive grain refinement in the high-strength

Al-Mg-Sc alloy containing coherent $Al_3(Sc,Zr)$ dispersoids resulted in a strong increase in the amplitude of serrations, similar to the observations on an Al-5.5 pct Mg alloy containing incoherent nanoscale Al_6Mn dispersoids,[26] and led to a change in the commonly observed sequence of types of PLC behavior (Figures 3, 4, 5, 8). These observations are conform to the general understanding that on the one hand, the second-phase particles can strongly modify the conditions for DSA,[56] and on the other hand, the mechanisms of interaction of mobile dislocations with incoherent or coherent dispersoids are distinctly different.[57]

From engineering point of view, the microstructural conditions allowing for suppression of plastic instability are of great interest. The formation of a fully recrystallized structure containing a large dislocation density (Table I) was found to hinder the formation of slip features on the surface of Al-Mg-Sc, thus improving the surface roughness. In addition, grain refinement suppresses the formation of strong surface markings that otherwise occur in the necked region. It can be expected that the grain refinement may eliminate the striated surface topology that is caused by the PLC effect. Moreover, it is worth noting that the surface roughness remains relatively low if an Al-Mg alloy exhibiting DSA is subjected to tension up to the onset of necking. Thus, the extensive grain refinement may be rather effective for improving roughness in the necked region.

Concurrently, the extensive grain refinement deeply changes tensile deformation behavior. In the reference deformation conditions, in particular, a transition to a well-defined yielding plateau and high-amplitude type B serrations takes place by increasing the volume fraction of recrystallized grains. Similar mechanical behavior was exhibited by a Zr-modified AA5083 alloy[26] and a AA5182 alloy with fully recrystallized structure[58] and average grain sizes of 1 and 11 μm, respectively.

V. CONCLUSIONS

1. The 5024 alloy tested in the coarse-grained condition exhibits usual behavior of the PLC effect in the temperature interval from 223 K to 348 K (from $-50\,^{\circ}$C to $75\,^{\circ}$C). Type $A + B$ serrations are observed at the reference conditions (298 K ($25\,^{\circ}$C) and $\dot{\varepsilon} = 10^{-3}\,\mathrm{s}^{-1}$) corresponding to the middle part of the temperature and strain rate domain of the PLC effect. Type C and A serrations take place at lower and higher strain rates, respectively. Similar behavior was found after 1 or 2 ECAP passes, leading to the formation of a well-defined subgrain structure with a little fraction of high-angle boundaries.
2. The formation of a partially or fully recrystallized micron-scale grain structure strongly affects mechanical behavior. Plastic deformation begins with a yielding plateau superimposed with deep type B serrations, which start practically at the yield point and last till fracture. At the reference conditions, which correspond to the least ε_c value in this state of the material, only type B behavior takes place. Surprisingly, the serration types which usually come along with the deformation band propagation are found not only near the high strain rate/low-T boundary of the PLC effect but also close to its opposite boundary. Mixed type $A + B$ shows up when approaching the left border (high temperatures) of the PLC domain, and type A serrations are observed at the right border (low temperatures). In contrast with the alloy containing a subgrain structure, no transition from $A + B$ or A serration types to type B takes place in vicinity of the PLC domain boundaries. The alloy with a partially recrystallized structure exhibits pure type D serrations when approaching the upper border (high strain rates) of the PLC domain.
3. The amplitude of stress serrations in the coarse-grained state of AA5024 Al alloy and reference deformation conditions comprises about 5 MPa. They tend to grow with the increasing volume fraction of recrystallized grains and achieve about 20 MPa after 12 ECAP passes. At the reference conditions, the amplitude of oscillations is nearly independent of strain in the alloy with ultra-fine-grained structure, while in the alloy with coarse-grained structure, the amplitude increases with strain up to the peak stress and then decreases until failure.
4. Coarse slip bands evolve in the material in coarse-grained condition, as well as within the remnants of unrecrystallized grains in the alloy with partially recrystallized structures after the onset of necking. There is a great difference in surface markings in areas of coarse grains before and after the onset of necking. The grain refinement suppresses the formation of coarse slip features, enhances the uniformity of the dislocation glide, and eliminates the dramatic difference in the sample roughness between neck region and region of uniform tension. The decreasing temperature or increasing strain rate promotes localization of the dislocation slip without any sense with PLC domain.

REFERENCES

1. A. Portevin and F. LeChatelier: *C. R. Acad. Sci. Paris*, 1923, vol. 176, pp. 507–10.

2. A. Portevin and F. Le Chatelier: *Trans. ASST*, 1924, vol. 5, pp. 457–78.
3. H. Aboulfadl, J. Deges, P. Choi, and D. Raabe: *Acta Mater.*, 2015, vol. 86, pp. 34–42.
4. J.M. Robinson and M.P. Shaw: *Int. Mater. Rev.*, 1994, vol. 39, pp. 113–22.
5. H. Halim, D.S. Wilkinson, and M. Niewczas: *Acta Mater.*, 2007, vol. 55, pp. 4151–60.
6. I.J. Polmear: *Light Alloys. From Traditional Alloys to Nanocrystals*, 4th ed., Elsevier, Amsterdam, 2006, p. 421.
7. M.S. Bharathi, M. Lebyodkin, G. Ananthakrishna, C. Fressengeas, and L.P. Kubin: *Acta Mater.*, 2002, vol. 50, pp. 2813–24.
8. J. Kang, D.S. Wilkinson, M. Jain, J.D. Embury, A.J. Beaudoin, S. Kim *et al.*: *Acta Mater.*, 2006, vol. 54, pp. 209–18.
9. H. Neuhauser: in *Patterns, Defects and Material Instabilities*, D. Walgref and N.M. Ghoniem, eds., Kluwer Academic Publishers, Dordrecht, 1990, pp. 241–77.
10. Y. Estrin and L.P. Kubin: in *Continuum Models for Materials with Microstructure*, H.B. Muhlhaus, ed., Wiley, New York, 1995, pp. 395–450.
11. R.C. Picu: *Acta Mater.*, 2004, vol. 52, pp. 3447–58.
12. J. Balik and P. Lukac: *Acta Metall. Mater.*, 1993, vol. 41, pp. 1447–54.
13. M.R. Stoudt, J.B. Hubbard, M.A. Iadicola, and S.W. Banovic: *Metall. Mater. Trans. A*, 2009, vol. 40A, pp. 1611–22.
14. H. Louche, P. Vacher, and R. Arrieux: *Mater. Sci. Eng. A*, 2005, vol. 404, pp. 188–96.
15. H. Jiang, Q. Zhang, X. Chen, Z.H. Chen, Z.H. Jiang, X. Wu *et al.*: *Acta Mater.*, 2007, vol. 55, pp. 2219–28.
16. M.A. Lebyodkin and T.A. Lebedkina: *Phys. Rev. E*, 2008, vol. 77, p. 026111 1-8.
17. I.V. Shashkov, M.A. Lebyodkin, and T.A. Lebedkina: *Acta Mater.*, 2012, vol. 60, pp. 6842–50.
18. S.H. Zhao, Ch. Meng, F. Mao, W. Hu, and G. Gottstein: *Acta Mater.*, 2014, vol. 76, pp. 54–67.
19. W. Wen and J.G. Morris: *Mater. Sci. Eng. A*, 2004, vol. 373, pp. 204–16.
20. A. Sarkar, P. Barat, and P. Mukherjee: *Metall. Mater. Trans. A*, 2013, vol. 44A, pp. 2604–12.
21. M.A. Muñoz-Morris, C.G. Oca, and D.G. Morris: *Scripta Metall.*, 2003, vol. 48, pp. 213–18.
22. M.V. Markushev and M.Y. Murashkin: *Mater. Sci. Eng. A*, 2004, vol. 367, pp. 234–42.
23. T.A. Lebedkina, M.A. Lebyodkin, T.T. Lamark, M. Janeček, and Y. Estrin: *Mater. Sci. Eng. A*, 2014, vol. 615, pp. 7–13.
24. R. Kapoor, C. Gupta, G. Sharma, and J.K. Chakravartty: *Scripta Mater.*, 2005, vol. 53, pp. 1389–93.
25. M. Wagenhofer, M. Erickson-Natishan, R.W. Armstrong, and F.J. Zerilli: *Scripta Mater.*, 1999, vol. 41, pp. 1177–84.
26. S. Malopheyev and R. Kaibyshev: *Mater. Sci. Eng. A*, 2014, vol. 620, pp. 246–52.
27. P. Fernandez-Zelaia, B.S. Adair, V.M. Barker, and S.D. Antolovich: *Metall. Mater. Trans. A*, 2015, vol. 46A, pp. 5596–609.
28. D.A. Zhemchuzhnikova, M.A. Lebyodkin, T.A. Lebedkina, and R.O. Kaibyshev: *Mater. Sci. Eng. A*, 2015, vol. 639, pp. 37–41.
29. A. Mogucheva, E. Babich, B. Ovsyannikov, and R. Kaibyshev: *Mater. Sci. Eng. A*, 2013, vol. 560, pp. 178–92.
30. R.Z. Valiev and T.G. Langdon: *Prog. Mater. Sci.*, 2006, vol. 51, pp. 881–981.
31. R. Schwab and V. Ruff: *Acta Mater.*, 2013, vol. 61, pp. 1798–808.
32. C.Y. Yu, P.W. Kao, and C.P. Chang: *Acta Mater.*, 2005, vol. 53, pp. 4019–28.
33. S.D. Antolovich and R.W. Armstrong: *Prog. Mater. Sci.*, 2014, vol. 59, pp. 1–160.
34. T.A. Lebedkina and M.A. Lebyodkin: *Acta Mater.*, 2008, vol. 56, pp. 5567–74.
35. R. Král and P. Lukáč: *Mater. Sci. Eng. A*, 1997, vols. 234–236, pp. 786–89.
36. A.H. Cottrell: *Philos. Mag.*, 1953, vol. 44, pp. 829–32.
37. M.A. Lebyodkin, Y. Brechet, Y. Estrin, and L.P. Kubin: *Phys. Rev. Lett.*, 1995, vol. 74, pp. 4758–61.
38. P.S. Lee, H.R. Piehler, B.L. Adams, G. Jarvis, H. Hampel, and A.D. Rollett: *J. Mater. Process. Technol.*, 1998, vols. 80–81, pp. 315–19.
39. M. Jain, D.J. Lloyd, and S.R. Macewen: *Int. J. Mech. Sci.*, 1996, vol. 38, pp. 219–32.
40. Y.S. Choi, H.R. Piehler, and A.D. Rollett: *Metall. Mater. Trans A*, 2004, vol. 35A, pp. 513–24.
41. S. Raj and T. Langdon: *Acta Metall. Mater.*, 1991, vol. 39, pp. 1817–22.
42. J. Kang, D.S. Wilkinson, J.D. Embury, M. Jain, and A.J. Beaudoin: *Scripta Mater.*, 2005, vol. 53, pp. 499–503.
43. R. Kaibyshev, O. Sitdikov, A. Goloborodko, and T. Sakai: *Mater. Sci. Eng. A*, 2003, vol. 344, pp. 348–56.
44. A. Pineau: *Philos. Trans. R. Soc. A*, 2015, vol. 373, p. 20140131, DOI:10.1098/rsta.2014.0131.
45. V. Bata and E.V. Pereloma: *Acta Mater.*, 2004, vol. 52, pp. 657–65.
46. I.A. Ovid'ko, A.G. Sheinerman, and R.Z. Valiev: *Scripta Mater.*, 2014, vol. 76, pp. 45–48.
47. R.Z. Valiev, N.A. Enikeev, M.Yu. Murashkin, V.U. Kazykhanov, and X. Sauvage: *Scripta Mater.*, 2010, vol. 63, pp. 949–52.
48. P. Hahner: *Acta Mater.*, 1997, vol. 45, pp. 3695–707.
49. L.P. Kubin and Y. Estrin: *Acta Metall. Mater.*, 1990, vol. 38, pp. 697–708.
50. S.H1. Fu, T. Cheng, Q. Zhang, Q. Hu, and P. Cao: *Acta Mater.*, 2012, vol. 60, pp. 6650–56.
51. J. Røyset and N. Ryum: *Int. Mater. Rev.*, 2005, vol. 50, pp. 19–44.
52. M. Jobba, R.K. Mishra, and M. Niewczas: *Int. J. Plast.*, 2015, vol. 65, pp. 43–60.
53. B. Tian: *Mater. Sci. Eng. A*, 2003, vol. 349, pp. 272–78.
54. H. Ait-Amokhtar, S. Boudrahema, and C. Fressengeas: *Scripta Mater.*, 2006, vol. 54, pp. 2113–18.
55. J. Kang, R.K. Mishra, D.S. Wilkinson, and O.S. Hopperstad: *Philos. Mag. Lett.*, 2012, vol. 92, pp. 647–55.
56. Y. Estrin and M.A. Lebyodkin: *Mater. Sci. Eng. A*, 2004, vols. 387–389, pp. 195–98.
57. E. Nembach: *Particle Strengthening of Metals and Alloys*, Wiley, New York, 1996.
58. R. Nogueira de Codes, O.S. Hopperstadt, O. Engler, O.G. Lademo, J.D. Embury, and A. Benallal: *Metall. Mater. Trans. A*, 2011, vol. 42A, pp. 3358–69.